Journal of Cleaner Production 369 (2022) 133352

Contents lists available at ScienceDirect

Journal of Cleaner Production

journal homepage: www.elsevier.com/locate/jclepro

The bond strength of reinforced concrete with confinement of recycled steel strap

Muhd Fauzy Sulaiman [a], Chee-Loong Chin [b], Chau-Khun Ma [b,c,*], Abdullah Zawawi Awang [b], Wahid Omar [b]

[a] Department of Irrigation and Drainage (Federal Territory of Labuan), Ministry of Environment and Water, Malaysia
[b] Department of Structures and Materials, School of Civil Engineering, Faculty of Engineering, Universiti Teknologi Malaysia, Malaysia
[c] Forensic Engineering Centre, Institute for Smart Infrastructure and Innovative Construction, School of Civil Engineering, Faculty of Engineering, Universiti Teknologi Malaysia, Malaysia

ARTICLE INFO

Handling Editor: Zhen Leng

Keywords:
Recycled steel
Bond strength
Active confinement
Prestressed confinement
Structural strengthening

ABSTRACT

The potential use of recycled steel strap from packaging industry to strengthen bond between reinforcement steel and concrete was investigated. Through a series of pull-out experimental tests, this technique was shown to improve the bond properties between reinforcement steel and concrete. This research found that concrete strength and amount of steel straps provided for confinement affect the improvements on the bond between reinforcement steel and concrete. The analysis conducted in this research found that higher concrete strength and less amount of steel strap confinement would result in lower improvement in the bond strength. Subsequently, the effects of concrete strength and amount of steel strap confinement provided were considered into a newly developed equation to estimate bond strength. This research also conducted a model assessment on the proposed equation and the equation was found to be in good agreement with the experimental test results.

1. Introduction

Construction of new reinforced concrete (RC) buildings contributes a great share of global carbon emissions (Olivier et al., 2012). With the increase in world population, the demand for more RC buildings will increase leading to large global carbon emission. In recent years, United Nations Environment Programme (United Nations Environment Programme, 2020) and Chan et al. (2020) highlighted huge potential for reuse of structures and buildings in their end of services. This strategy can prolong the usefulness of the structures, leading to an overall reduction in the potential environmental damage (Chan et al., 2020; Conejos et al., 2014). Despite this, the lack of confidence on the structural properties of these structure has remains as a barrier to reuse of these structures (Iacovidou and Purnell, 2016). One of the most important structural properties of concerned that governs the performance of RC structures is the bond between concrete and reinforcement steel (CEB-FIP, 1995; Sulaiman et al., 2017). Poor bond or insufficient bond between concrete and reinforcement steel can cause slipping of reinforcement steel and cripple the ability of RC structure to develop their full flexural strengths and ductility (Choi et al., 2013). This can lead to excessive deflection, cracks, or collapse of the entire RC structure.

For ribbed reinforcement bar, the bond strength is primarily governed by the mechanical interlock between the concrete and the ribs on the surface of the reinforcement (Kaklauskas et al., 2017). With higher bond strength, the bond length required in anchorage for development of full reinforcement strength can be reduced. Previous research showed that such bond can be improved by introducing steel fibre to the concrete mix (Chu and Kwan, 2021) or by providing more confining reinforcement (Bamonte and Gambarova, 2007). The addition of steel fibre in steel fibre reinforced concrete (SFRC) was able to provide some confining effect to the concrete and restrain the widening of cracks when the steel reinforcement is subjected to load (Chu and Kwan, 2021; Bandelt et al., 2017). This was reported to be able to improve the crack control or crack mitigation properties of RC structure (Chu and Kwan, 2021). Besides, SFRC also has superior mechanical properties as compared to conventional concrete, including compressive strength, tensile strength, toughness, and others (Chu et al., 2018). Nonetheless, since this addition of steel fibre involve mixing the steel fibre into the concrete matrix, it is more suitable to be implemented for construction

* Corresponding author. Department of Structures and Materials, School of Civil Engineering, Faculty of Engineering, Universiti Teknologi Malaysia, Malaysia.
E-mail addresses: cheeloong.chin@utm.my (C.-L. Chin), machaukhun@utm.my (C.-K. Ma).

https://doi.org/10.1016/j.jclepro.2022.133352
Received 4 May 2021; Received in revised form 18 July 2022; Accepted 24 July 2022
Available online 1 August 2022

of new RC structures. For strengthening of existing RC structure, the use of external confinement to increase the bond strength is more viable (Choi et al., 2013; Hamad et al., 2005; Torre-Casanova et al., 2013; Ong et al., 2022). It was reported that external confinement can transfer sudden splitting failure to ductile pull-out failure of bond. This provides sufficient warning signs prior to failure and is favourable in structural engineering. Besides, external confinement can increase strength, flexural capacity, and ductility of RC structures (Ma et al., 2016a; Alagusundaramoorthy et al., 2003; Chin et al., 2019a). Zhang et al. (2020) reported that shear capacity of the concrete column can be improved with steel tube confinement. Wang et al. (2021) investigated the use of both fiber reinforced polymer (FRP) and steel tube to confine concrete column. It was shown that the external confinement was able to significantly improve the axial compressive behaviour. Together with the flexibility of installation, external confinement is a potential solution to improve the structural properties of existing structures (Ong et al., 2022). With sufficient improvement on the structural properties of existing structures, more structures can be reused with higher confidence.

Recent research revealed that recycled steel strap (RSS) from packaging industry can be used to provide prestressed or active confinement to concrete (Awang, 2013). This active RSS confinement can achieve better confinement effectiveness and can divert the wastes from packaging industry to construction industry (Ma et al., 2016b; Yang et al., 2019; Moghaddam et al., 2010). In previous research, Moghaddam et al. (2010) reported significantly higher improvements of strength and ductility using active confinement compared to those of passive confinement under the same confinement configuration. Subsequently, Awang (2013) introduced a new technique that allowed the use of multiple layers RSS confinement to apply active confinement on high strength concrete (HSC). Chin et al. (2019b) reported that higher prestressing level can result in higher strength and improved elastic limit. Recently, Yang et al. (2019) showed that active RSS confinement can improve the ductility and energy dissipation of RC beam-column joint deficient of current design codes. Active RSS confinement can also be used on non-circular section despite having a reduce effectiveness (Chin et al., 2020).

A recent review conducted by the author highlighted that bond strength can be significantly improved using active confinement (Sulaiman et al., 2017). However, there is very limited experimental evidence of using active RSS confinement to improve the bond strength. Hence, it is not empirically known whether active RSS confinement can improve the bond strength. Moreover, the expressions for bond strength in current design codes were calibrated using experimental results of normal strength concrete (NSC) only and may not be suitable for HSC. Besides, the effect of active RSS confinement is not being quantified in the design codes. Therefore, this study aims to investigate the improvement provided by active RSS confinement to the bond strength between concrete and reinforcement steel. This study first presents an experimental test related to bond strength in NSC and HSC under active RSS confinement. Subsequently, this suitability of expressions for bond strength in existing design codes is assessed using the results of experimental test. In the last part of this study, a new expression to estimate bond strength in NSC and HSC under active RSS confinement is proposed to be included in design codes.

2. Experimental preparation

In this study, two types of concrete were used to represent NCS and HSC. The 28-day strengths of NSC and HSC were designed to be 30 MPa and 60 MPa, respectively based on British Concrete Mix Design approach. The concrete mix proportions are tabulated in Table 1. The cement used was Type I Portland Cement according to ASTM C150 (ASTM C150, 2020). The water used was tap water. The fine aggregate used in this research was well graded river sand. The coarse aggregates used was well graded crushed stones with 10-mm nominal size. MIGHTY 21 polycarboxylate ether high-range water reducer was used as the superplasticizer.

Reinforcement bars used in this study were 12 mm and 16 mm diameter deformed reinforcement bar with a yield stress of 526 MPa and tensile strength of 621 MPa. The reinforcement was cut to 700 mm long. A total length of 300 mm of reinforcement bar was embedded in concrete. The bond length was designed to be $5d_b$. To achieve this, two PVC tubes with 15 mm diameter and 120 mm length were used as debonding tubes to sheath the reinforcement steel from concrete. Fig. 1 shows the preparation of bond length in this experiment.

PVC tube with 150 mm diameter and 300 mm length were used as the formwork of the specimens. The reinforcement bar was placed and casted at the centre of the formwork as illustrated in Fig. 2. The selective of cylindrical specimen instead of cubic is to provide axisymmetric cover to reinforcement (Orangun et al., 1977). Formwork oil was applied on the internal surface of the 150 mm diameter PVC tube before casting. During casting, the concrete was poured in three layers and each layer was compacted by using poker vibrator. The formwork was covered with wet burlap cloth and the concrete was left for curing. The formwork was removed seven days after casting. Subsequently the specimens were covered by wet burlap cloth for curing. Compression tests were conducted on 28 days after casting in accordance with BS EN 12390–3:2009 (British Standards Institution, 2009) on three companion concrete cubes of NSC and three companion cubes of HSC. The average concrete cube strengths were 40.30 MPa for NSC and 60.50 MPa for HSC.

The RSS used in this study was obtained from packaging industry. It has width of 15 mm, thickness of 0.5 mm, and yield stress of 805 MPa. The RSS was cut into desired length and was made into confinement hoops and connections clips as shown in Fig. 3. The length of internal anchorage and prestressing end were set to 100 mm, similar to a recent research (Chin et al., 2019b).

The specimens were confined with the RSS confinement hoop and

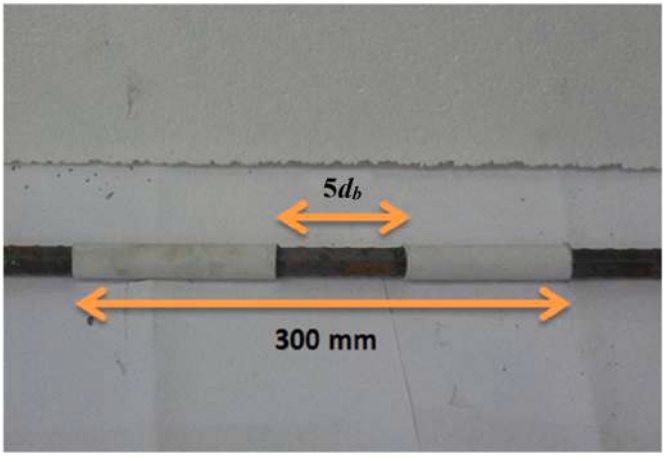

Fig. 1. Bond length in reinforcement.

Table 1
Concrete mixes for NSC and HSC.

Concrete Mix	Cement (kg/m^3)	Water (kg/m^3)	Fine Aggregates (kg/m^3)	Coarse Aggregates (kg/m^3)	Superplasticizer (L/m^3)	Slump (mm)
NSC	472	250	720	878	–	110
HSC	515	170	645	1100	6.2	170

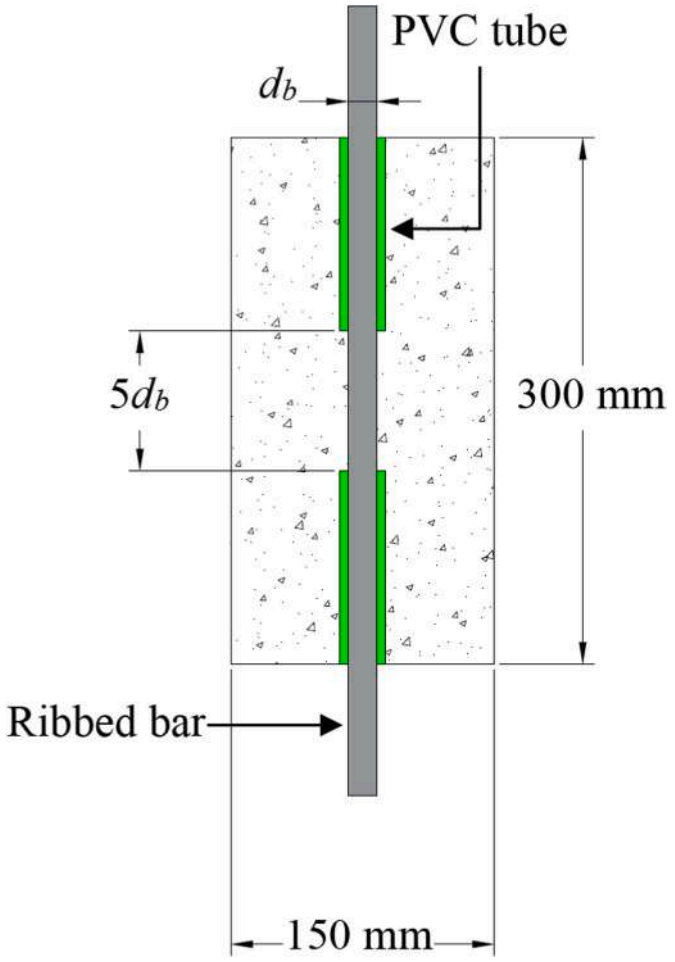

Fig. 2. Schematic diagram of pull-out specimen.

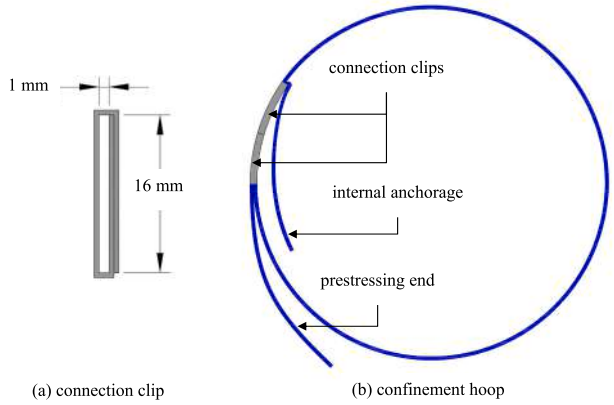

Fig. 3. Confinement details.

prestressed using a pneumatic tensioner. The air pressure supplied to the pneumatic tensioner was set to 0.3 MPa. The prestressing force was applied to the prestressing end. Subsequently the prestressing end was mechanically anchored and locked to the connection clips. An illustration of the confining and prestressing technique is presented in Fig. 4. The specimens were confined with four different configurations by adjusting the spacings between each strap of RSS. Fig. 5 shows the confinement configurations used in this study.

Each specimen is designated using the following convention: [specimen type]-[sample number]-[concrete strength]. For instance, SS0-1-G60 indicates of no spacing, one out of two specimens, and concrete strength of 60 MPa. The confinement ratio was calculated by using Eq. (1) proposed by Awang (2013). The detail of each specimen group was shown in Table 2.

$$\rho_v = \frac{f_y V_s}{f_c V_c} = \frac{4wtf_y}{s_{cl} D f_c} \tag{1}$$

where ρ_v is confinement ratio; f_c is concrete cubic compressive strength; f_y is yield stress of RSS; V_s is volume of RSS; V_c is volume of concrete; D is diameter of concrete; t is thickness of RSS; s_{cl} is clear spacing between RSS; and w is width of RSS.

3. Experimental test setup

The pull-out test was carried out at Structures and Materials Laboratory, Universiti Teknologi Malaysia by using Universal Testing Machine with rated capacity of 2000 kN. Initially, the specimen was placed above hollow cylindrical base inside a specifically made steel frame located in the testing machine. A metal plate was then placed on top of the specimen to restraint it to the steel frame as shown in Fig. 6. A straight steel was attached to the reinforcement bar to translate the slip of reinforcement bar to a linear variable differential transformer (LVDT) with a gauge length of 100 mm. The slip measurement is required as to determine the bond strength of embedded bar correspond to slip of reinforcement (Sulaiman et al., 2017). The load cell and LVDT were connected to a data logger. The pull-out test was conducted in accordance to CEB-FIP (CEB-FIP, 1990) guideline procedure with a displacement controlled rate of 1.2 mm/min. A schematic diagram of the test setup is illustrated in Fig. 7.

Chu and Kwan (2018) highlighted that conventional pull-out test setup would overestimate the bond strength due to the confining effect arises from the friction between the metal plate and concrete. It was suggested to include soft rubber pad and low friction polytetrafluoroethylene film in between the metal plate and concrete to minimize the unintended frictional confining effect. Recent experimental tests adopted the idea to reduce the friction by including a soft friction reduction layer between the metal plate and concrete (Wei et al., 2019; Xiong et al., 2021). The fundamental behind this is to minimize the frictional confining effect near the bond region. In this research, the confining effect is minimized by increasing the distance between end plate to the bond region. This is in accordance with the concept of effective confinement used by Mander et al. (1988) where the effective confining region is projected at an angle of 45°. This reflects that the region affected by the frictional confining effect is only within $D/2$ distance from the contact surface as illustrated in Fig. 8(a).

To further validate this, an axisymmetric finite element analysis was conducted based on Cont-1-G60-16-80 to determine the region affected by the frictional confinement. The concrete, reinforcement bar and steel plate were modelled using 4-node bilinear axisymmetric quadrilateral element with reduced integration and hourglass control (CAX4R). In this analysis, the concrete was assumed to be linearly elastic with an elastic modulus of 36 GPa and Poisson's ratio of 0.18; the reinforcement bar and steel plate were assumed to be linearly elastic with an elastic modulus of 200 GPa and Poisson's ratio of 0.3. The nominal mesh size was set to 10 mm. All the contact surfaces were considered as perfect contact with no lack of fit and no slip using tie constraint. The boundary condition of the top of the steel plate was set to be pinned and no displacement was allowed. A pull force of 100 kN was applied on the reinforcement steel. Since a region is considered as confined when all three of its principal stresses are in compression. Therefore, negative maximum principal stress also indicates that the region is affected by confinement effect. Fig. 8(b) shows the distribution of maximum principal stress in the concrete. For ease of visualization, only the region with negative maximum principal stress was shaded with rainbow tone. As seen from the figures, the bonded region is far away and is not within

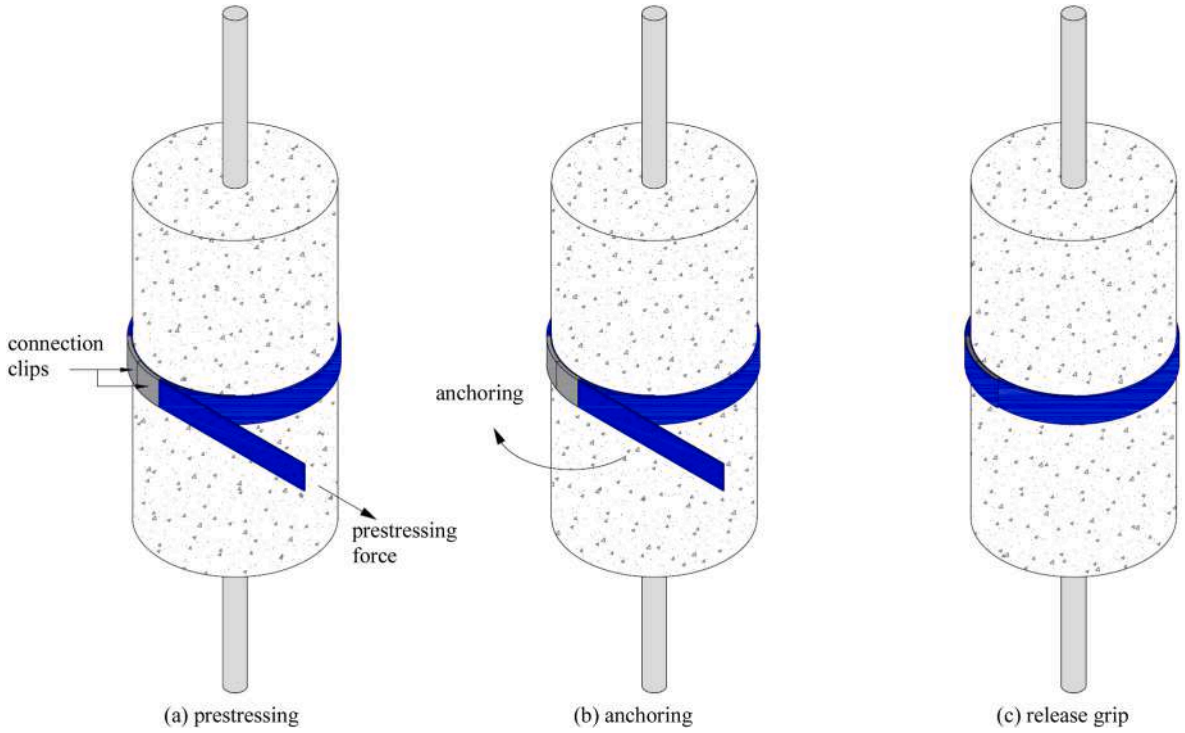

Fig. 4. Confining and prestressing technique.

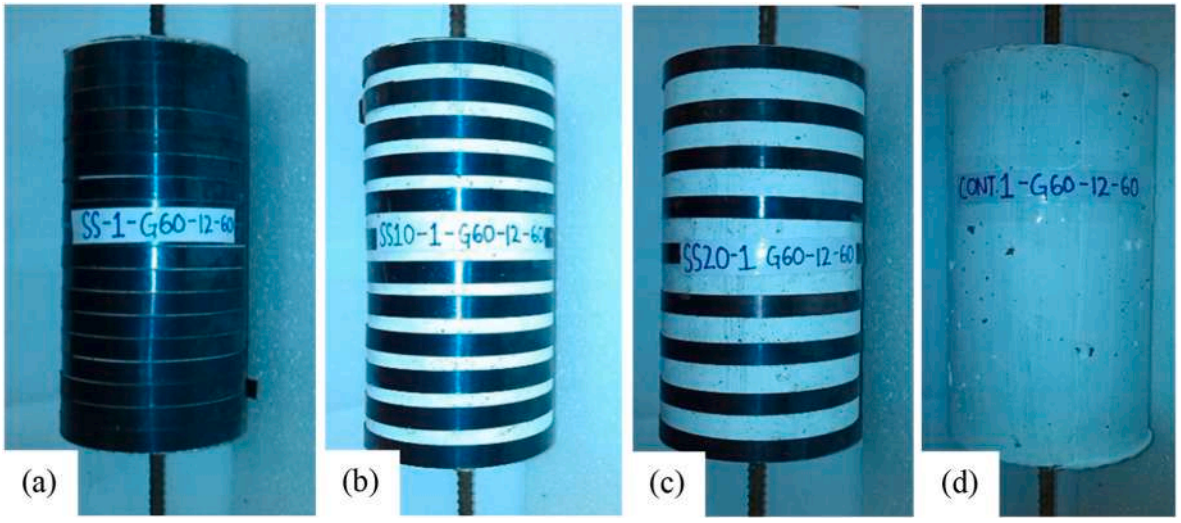

Fig. 5. Confinement configurations: (a) 0 mm spacing; (b) 10 mm spacing; (c) 20 mm spacing; and (d) no confinement.

the vicinity of the frictional confinement effect. Therefore, the setup used in this research is said to be not affected by the frictional confinement effect.

4. Results and discussion

There were two main failure modes observed during the experimental test, i.e., sudden splitting failure and slip induced splitting failure. These two failure modes are differentiated from the onset of concrete splits and does not remain sufficiently intact for bond. Fig. 9(a) shows an example of sudden splitting failure observed in this experimental test. This failure mode means that the concrete splits before the reinforcement steel slips. This failure mode is not desirable due to the lack of sufficient warning sign prior to the failure. Fig. 9(b) shows an example of slip induced splitting failure observed in this experimental test. This failure mode means that the concrete splits after the reinforcement steel slips. This type of failure is desirable since sufficient warning sign can be observed when the reinforcement steel slips.

Table 3 tabulated the bond strength and failure modes obtained from the experimental tests. The bond strength was calculated using Eq. (2). In the table, $\tau_{average}$ refers to average τ of each pair of identical specimens. $\tau_{cont,average}$ refers to $\tau_{average}$ of the specimens with no confinement.

$$\tau = \frac{P_{max}}{\pi d_b l_d} \tag{2}$$

where τ is bond strength; and P_{max} is the maximum load applied during the experimental test.

Both Cont-G60-12-60 and Cont-G60-16-80 sets exhibited sudden

Table 2
Specimens confinement ratio.

Designation	f_c (MPa)	s_{cl} (mm)	ρ_v
Cont-1-G40-12-60	40.3	–	0.000
Cont-2-G40-12-60	40.3	–	0.000
SS20-1-G40-12-60	40.3	20	0.114
SS20-2-G40-12-60	40.3	20	0.114
SS10-1-G40-12-60	40.3	10	0.160
SS10-2-G40-12-60	40.3	10	0.160
SS0-1-G40-12-60	40.3	0	0.266
SS0-2-G40-12-60	40.3	0	0.266
Cont-1-G60-12-60	60.5	–	0.000
Cont-2-G60-12-60	60.5	–	0.000
SS20-1-G60-12-60	60.5	20	0.076
SS20-2-G60-12-60	60.5	20	0.076
SS10-1-G60-12-60	60.5	10	0.106
SS10-2-G60-12-60	60.5	10	0.106
SS0-1-G60-12-60	60.5	0	0.177
SS0-2-G60-12-60	60.5	0	0.177
Cont-1-G60-16-80	60.5	–	0.000
Cont-2-G60-16-80	60.5	–	0.000
SS20-1-G60-16-80	60.5	20	0.076
SS20-2-G60-16-80	60.5	20	0.076
SS10-1-G60-16-80	60.5	10	0.106
SS10-2-G60-16-80	60.5	10	0.106
SS0-1-G60-16-80	60.5	0	0.177
SS0-2-G60-16-80	60.5	0	0.177

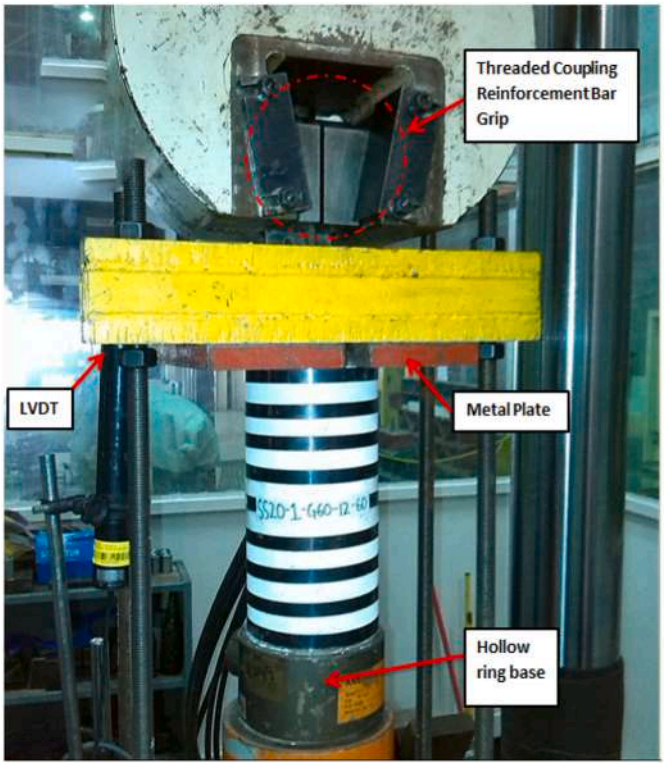

Fig. 6. Pull-out test arrangement.

splitting failure mode. This was believed to be inherited from the brittleness associated with the higher concrete strength. With the provision of active RSS confinement, this sudden splitting failure mode was changed to slip induced splitting failure mode as exhibited by other confined G60 specimens. This improvement on failure mode was also reported by previous study where higher confining pressure gradually changed the splitting failure to pull-out bond failure (Torre-Casanova et al., 2013).

It can be noticed that bond strengths of Cont-G60 set are considerably higher than those of Cont-G40 set. This means that bond strength is

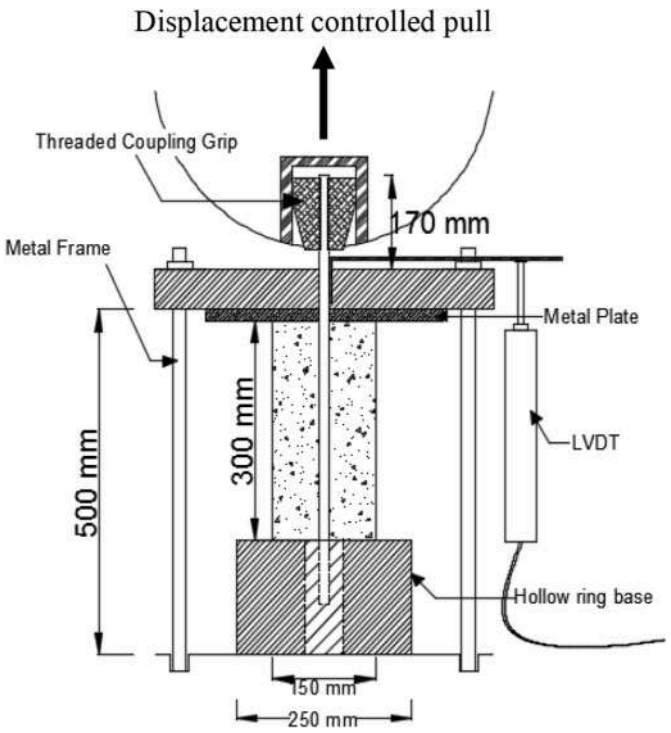

Fig. 7. Schematic diagram of pull-out test.

largely influenced by concrete strength. This is consistent with existing models (CEB-FIP, 1995; Orangun et al., 1977; ACI 408, 2003; Darwin et al., 1992) and previous experimental tests (Torre-Casanova et al., 2013; Lee et al., 2008). Hence, in this study the bond strengths of confined specimens are normalized with their respective control specimens to better show the effect of RSS confinement on bond strength.

Fig. 10 shows three plots of $\tau/\tau_{cont,average}$ against f_c, ρ_v and d_b. It can be observed that $\tau/\tau_{cont,average}$ is more correlated with f_c and ρ_v and less correlated to d_b from the correlation factors, R^2. This indicates that the efficiency of RSS confinement is affected by f_c and ρ_v, but not d_b. The downward trends shown in Fig. 10(a) reflects that efficiency of RSS confinement decreases as f_c increases. This is expected because efficiency of every type of confinement was found to be less pronounced when f_c increases (Lee et al., 2008; Chin et al., 2018; Samani and Attard, 2012; Lim and Ozbakkaloglu, 2014). Fig. 10(b) show that $\tau/\tau_{cont,average}$ increases when ρ_v increases. Higher ρ_v can ensure higher increment in bond strength between reinforcement steel and concrete. This is because higher ρ_v can provide higher confining pressure to the concrete (Zhang et al., 2020). This translates to higher contact pressure applied to the reinforcement bar. This tightens the bond between concrete and reinforcement steel and therefore leads to higher bond strength (Torre-Casanova et al., 2013; Gong et al., 2021). Fig. 10(c) shows that $\tau/\tau_{cont,average}$ decreases when d_b increases. However, the R^2 is low and therefore no significant inference can be made. These highlights that f_c and ρ_v should be included in the expression for bond strength to consider the effect of RSS confinement.

The bond slip relations of G40-12-60 specimens are plotted in Fig. 11 (a). As evidenced from the figure, RSS confinement can significantly improve the maximum slip exhibited by the specimens. For instance, the maximum slip exhibited by SS0-G40-12-60 was 13.3 mm while the maximum slip exhibited by Cont-G40-12-60 was 1.64 mm. It is noted that for Cont-G40-12-60, the bond failed prematurely promptly after reaching the peak stress leading to the small slip recorded at the peak stress. The experimental result showed that RSS confinement improved the maximum slip from 1.64 mm to 13.3 mm which represents an improvement of about 700%. This large improvement revealed that RSS confinement has huge potential to improve the ductility of RC

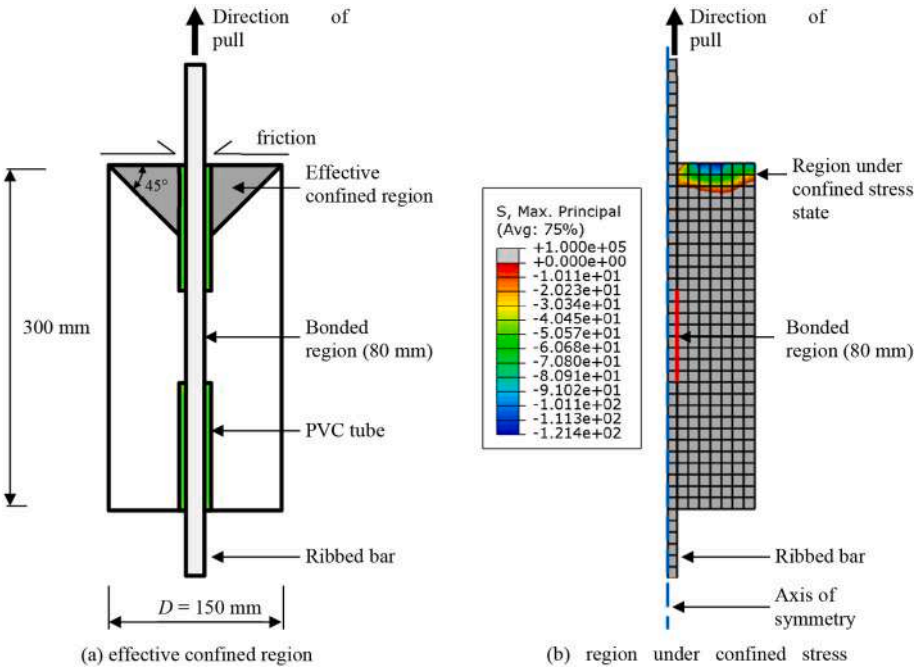

Fig. 8. Region affected by the frictional confining effect.

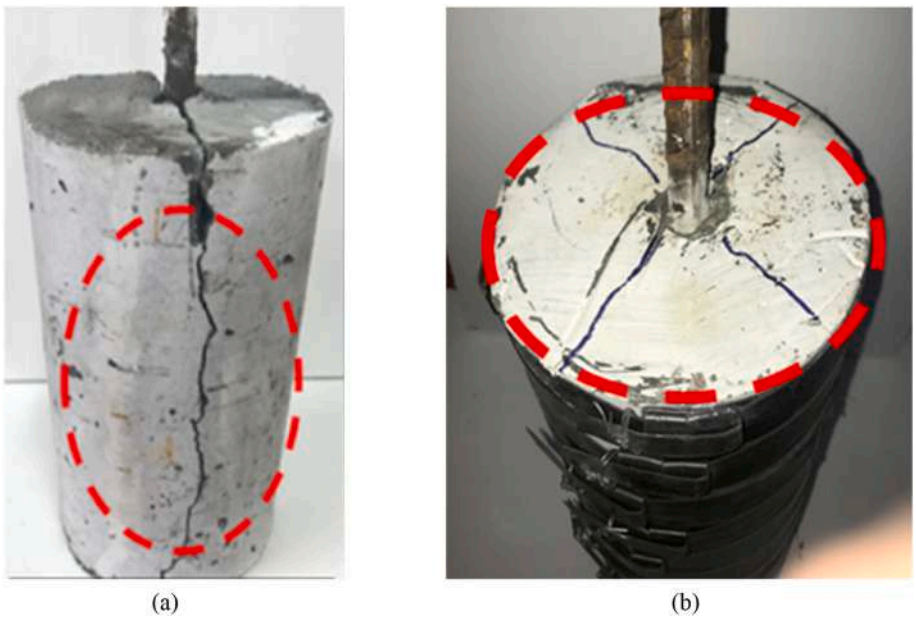

Fig. 9. Typical failure modes: (a) sudden splitting; and (b) slip induced splitting.

structures.

Fig. 11(b) shows the bond slip relation of G60-12-60 specimens. It is evidenced that RSS confinement can improved the maximum slip of G60-12-60 specimens. Comparison between Cont-G60-12-60 and SS0-G60-12-60 specimens showed that RSS confinement can improve the maximum slip from 6.38 mm to 10.95 mm. This represents an improvement of about 72%. The lower improvement in maximum slip of G60-12-60 specimens compared to those of G40-12-60 specimens is mainly due to the inherent brittleness associated with the higher concrete strength. Besides, this phenomenon suggested that higher confinement ratio is necessary to improve the ductility of HSC.

From the bond-slip relationships, it can be concluded that the curves consisted of two stages. In the first stage, adhesion and friction were responsible to resist the pull-out and to transfer the tensile stresses to surrounding concrete. This stage ends when the specimens reached their respective friction bond limit in which the friction is significantly reduced. At the second stage, the mechanical interlocking between ribbed bar and surrounding concrete was responsible to resist the pull-out and to transfer tensile stresses to surrounding concrete. At this stage, the presence of RSS confinement holds the concrete core to retains its integrity. Sufficient RSS confinement was shown to be capable of significantly delay the failure of the bond.

5. Comparison with existing models

The experimental test results were compared with existing bond

Table 3
Experimental bond strength and failure modes.

Specimen ID	Bond Strength, P_{max} (kN)	τ (MPa)	$\tau_{average}$ (MPa)	$\frac{\tau}{\tau_{cont,\ average}}$	Failure Mode[a]
Cont-1-G40-12-60	41	18.13	17.02	1.06	B
Cont-2-G40-12-60	36	15.92		0.94	B
SS20-1-G40-12-60	52	22.99	22.33	1.35	B
SS20-2-G40-12-60	49	21.66		1.27	B
SS10-1-G40-12-60	48	21.22	22.54	1.25	B
SS10-2-G40-12-60	54	23.87		1.40	B
SS0-1-G40-12-60	50	22.10	24.31	1.30	B
SS0-2-G40-12-60	60	26.53		1.56	B
Cont-1-G60-12-60	66	29.18	28.51	1.02	A
Cont-2-G60-12-60	63	27.85		0.98	A
SS20-1-G60-12-60	69	30.50	29.40	1.07	B
SS20-2-G60-12-60	64	28.29		0.99	B
SS10-1-G60-12-60	67	29.62	30.28	1.04	B
SS10-2-G60-12-60	70	30.95		1.09	B
SS0-1-G60-12-60	71	31.39	31.83	1.10	B
SS0-2-G60-12-60	73	32.27		1.13	B
Cont-1-G60-16-80	106	26.36	26.98	0.98	A
Cont-2-G60-16-80	111	27.60		1.02	A
SS20-1-G60-16-80	119	29.59	27.35	1.10	B
SS20-2-G60-16-80	101	25.11		0.93	B
SS10-1-G60-16-80	117	29.09	29.22	1.08	B
SS10-2-G60-16-80	118	29.34		1.09	B
SS0-1-G60-16-80	114	28.35	29.34	1.05	B
SS0-2-G60-16-80	122	30.33		1.12	B

[a] A refers to sudden splitting failure; and B refers to slip induced splitting.

strength models developed in the literature listed in Table 4. These models were used to estimate the bond strengths of each specimen tested in this study. It is noted that these models were developed and calibrated against various types of concrete, including plain concrete, transversely reinforced concrete, fibre reinforced concrete and transversely confined concrete.where $c_{min} = \min(c_y, c_s/2)$; c_y is the bottom concrete cover; c_s is distance between reinforcement bars; d_b is diameter of reinforcement bar; l_d is bond length of reinforcement bar; f_c is the concrete compressive strength; $c_{max} = \max(\min(c_x, c_s/2), c_y)$; c_x is side concrete cover; and $c = \min(c_s, c_y, c_s/2)$; $K_{tr} = n_{st}A_{tr}/(s\ d_b\ n_b)$; A_b is cross-sectional area of reinforcement bar; A_{st} is the cross-sectional area of the stirrups; $x =$ volume of fibre(length of fibre/diameter of fibre); and s is centre spacing of the stirrups.

Table 5 tabulates the estimations of bond strength on each specimen using existing models. In this table, τ_{model} represents bond strength estimated from model; and τ_{exp} represents bond strength obtained from experimental test. As evidenced from the table, these models perform reasonably well for Cont-1-G40 and Cont-2-G40. However, these models are over conservative in estimating bond strength of the specimens in

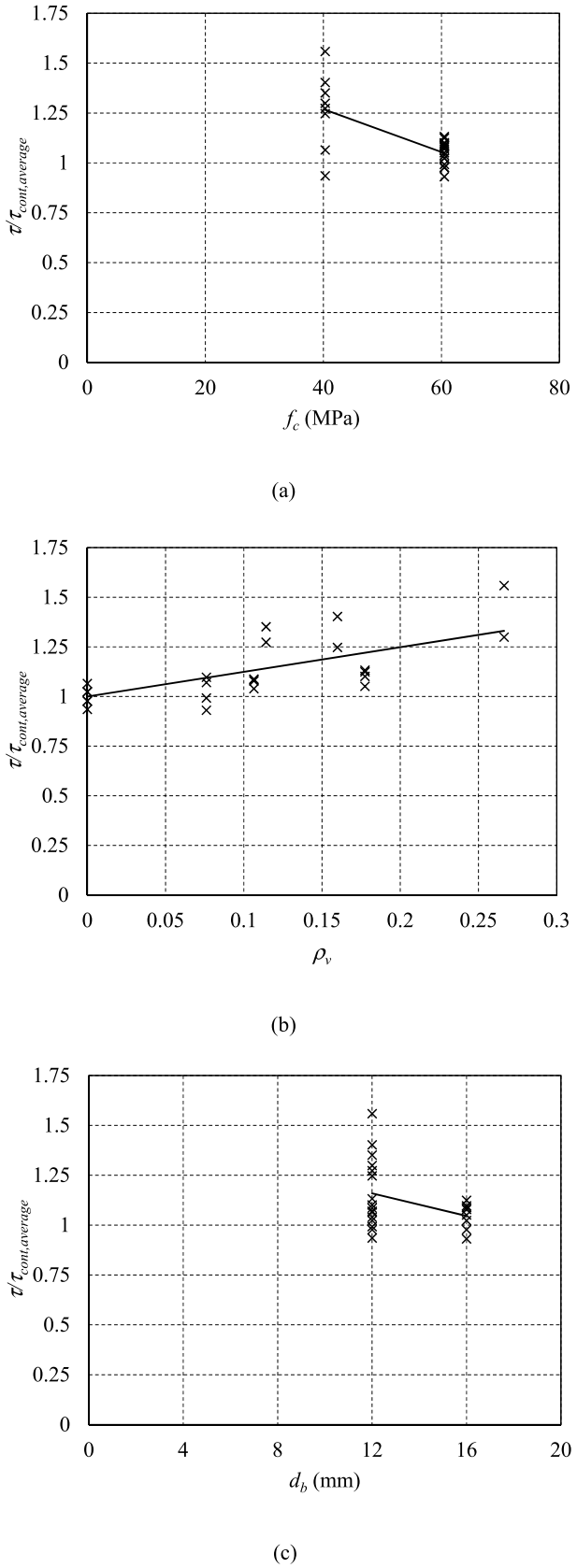

Fig. 10. Relationship of bond strength with: (a) f_c; (b) ρ_v; and (c) d_b.

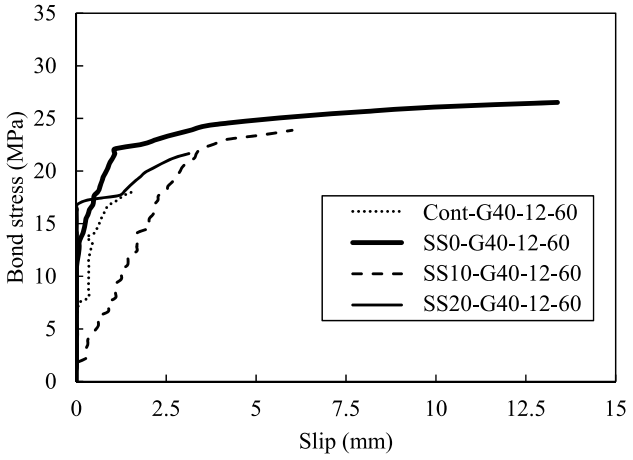

(a) G40-12-60 set

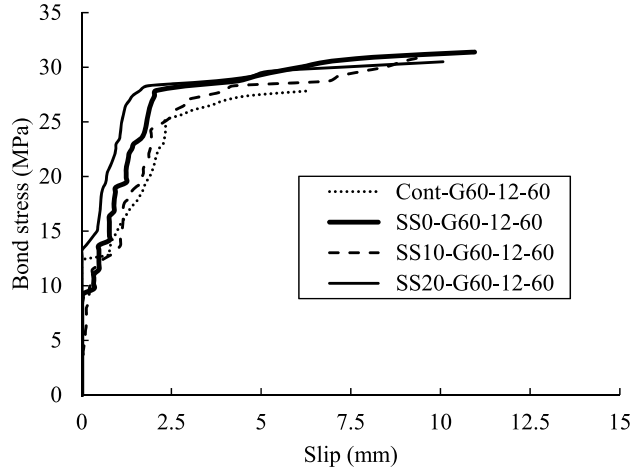

(b) G60-12-60 set

Fig. 11. Bond slip relation.

Table 4
Existing bond strength models.

Reference	Bond Strength Expression
Orangun et al. (1977)	$\tau = 0.083045\sqrt{f_c}\left[1.2 + 3\frac{c_{min}}{d_b} + 50\frac{d_b}{l_d}\right]$
Darwin et al. (1992)	$\tau = 0.083045\sqrt{f_c}\left[\left(1.06 + 2.12\frac{c}{d_b}\right)\left(0.92 + 0.08\frac{C^*_{max}}{C_{min}}\right) + 75\frac{d_b}{l_b}\right]$
ACI 408 (2003)	$\tau = \frac{[1.43l_d(c_{min} + 0.5d_b) + 57.4A_b]\left(0.1\frac{c_{max}}{c_{min}} + 0.9\right)f_c^{0.25}}{\pi d_b l_d}$
CEB-FIP (1995)	$\tau = 2.5\sqrt{f_c}$
Chu and Kwan (2019)	$\tau = 2.39(f_c)^{0.5}(1 + 0.072f_c x^{0.7})$
fib Bulletin 72 (2014)	$\tau = 13.5\left(\frac{f_c}{25}\right)^{0.25}\left(\frac{d_b}{l_b}\right)^{0.45}\left(\frac{25}{d_b}\right)^{0.2}\left[\left(\frac{c_{min}}{d_b}\right)^{0.25}\left(\frac{c_{max}}{c_{min}}\right)^{0.1} + 12K_{tr}\right]$

this experimental test. This can result in overdesigning the structures.

Fig. 12(a) shows the performance of existing models across the parameter f_c. It is shown that τ_{model}/τ_{exp} decreases below 1 when f_c increases. In particular, most of the τ_{model}/τ_{exp} for HSC specimens are below 0.75. This means that the existing models underestimate the bond strength in HSC by roughly 25%. Fig. 12(b) shows a plot of estimation/test ratio against ρ_v. It can be observed that most of the estimations/test ratios are below 0.75 when ρ_v is larger than 1. This indicates that the existing models are insufficient in estimating the bond strength in the presence of confinement.where τ_{model} is bond strength estimated from model; and τ_{exp} is bond strength obtained from experimental test.

To quantitatively assess the performance of these models, four statistical parameters are used in this study. Mean absolute error (MAE) given by Eq. (3) and mean squared error (MSE) given by Eq. (4) indicate the accuracy of the models. Lower MAE and MSE indicates higher accuracy. Linear trend slope (LTS) represents the slope of linear trend passing through the origin in the plot of τ_{model} against τ_{exp}. LTS near to 1 indicates that the trend of τ_{model} fits that of τ_{exp}. Hence, lower value of Eq. (5) represents better fit of trendline. Standard deviation (SD) given by Eq. (6) reflects the consistency of the estimations. Lower SD indicates higher consistency of the estimations.

$$\mathrm{MAE} = \frac{1}{N}\sum_{i=1}^{N}\left|\frac{\tau_{model,i}}{\tau_{exp,i}} - 1\right| \tag{3}$$

$$\mathrm{MSE} = \frac{1}{N}\sum_{i=1}^{N}\left(\frac{\tau_{model,i}}{\tau_{exp,i}} - 1\right)^2 \tag{4}$$

$$|1 - \mathrm{LTS}| = \left|1 - \frac{\sum_{i=1}^{N}\tau_{model,i}\tau_{exp,i}}{\sum_{i=1}^{N}{\tau_{exp,i}}^2}\right| \tag{5}$$

$$\mathrm{SD} = \sqrt{\frac{1}{N-1}\sum_{i=1}^{N}\left(\frac{\tau_{model,i}}{\tau_{exp,i}} - \frac{\overline{\tau}_{model,i}}{\overline{\tau}_{exp,i}}\right)^2} \tag{6}$$

where N is number of estimations; $\overline{\tau}_{model}$ is average of τ_{model}; and $\overline{\tau}_{exp}$ is average of τ_{exp}.

Fig. 13 shows the four statistical performances of existing models. From this figure, the statistical indicators showed that model proposed by CEB-FIP (CEB-FIP, 1995) has the best performance among these models. However, it is noted that this model lacks the consideration of confinement. For this reason, the general trend of this model is relatively poor with a LTS of 0.68. The model proposed by fib Bulletin 72 (fib Bulletin 72, 2014) achieved the second lowest MAE and MSE, rivalling the model proposed by CEB-FIP (CEB-FIP, 1995). The LTS of model proposed by fib Bulletin 72 (fib Bulletin 72, 2014) is also near to that of model proposed by CEB-FIP (CEB-FIP, 1995). The SD of model proposed by fib Bulletin 72 (fib Bulletin 72, 2014) is the highest among these models. This means that the consistency of Eq. model proposed by fib Bulletin 72 (fib Bulletin 72, 2014) is the lowest among these models. The model proposed by Chu and Kwan (2019) was shown to have the lowest SD among these models. This means that the model is the most consistent with the experimental test results.

From comparisons between experimental test results and existing models, it is shown that existing models need to be revised. The effect of confinement and effect of HSC on the bond strength have to be included and calibrated. With proper consideration of these effects, a larger portion of the benefits provided by RSS confinement can be exploited.

6. Proposed bond strength model

In this study, model proposed by fib Bulletin 72 (fib Bulletin 72, 2014) was adopted as the base form of model. This is because it is the only model that considered effect of confinement. A nonlinear regression analysis was conducted with the function given by Eq. (7). It is

Table 5
Performances of existing expressions for bond strength.

Specimens	τ_{exp} (MPa)	τ_{model} (MPa)						τ_{model}/τ_{exp}					
		Orangun et al. (1977)	Darwin et al. (1992)	ACI 408 (2003)	CEB-FIP (1995)	fib Bulletin 72 (2014)	Chu and Kwan (2019)	Orangun et al. (1977)	Darwin et al. (1992)	ACI 408 (2003)	CEB-FIP (1995)	fib Bulletin 72 (2014)	Chu and Kwan (2019)
Cont-1-G40-12-60	18.13	15.00	14.89	14.40	15.87	13.22	15.17	0.83	0.82	0.79	0.88	0.73	0.84
Cont-2-G40-12-60	15.92	15.00	14.89	14.40	15.87	13.22	15.17	0.94	0.94	0.90	1.00	0.83	0.95
SS20-1-G40-12-60	22.99	15.00	14.89	14.40	15.87	16.88	15.17	0.65	0.65	0.63	0.69	0.73	0.66
SS20-2-G40-12-60	21.66	15.00	14.89	14.40	15.87	16.88	15.17	0.69	0.69	0.66	0.73	0.78	0.70
SS10-1-G40-12-60	21.22	15.00	14.89	14.40	15.87	18.35	15.17	0.71	0.70	0.68	0.75	0.86	0.71
SS10-2-G40-12-60	23.87	15.00	14.89	14.40	15.87	18.35	15.17	0.63	0.62	0.60	0.66	0.77	0.64
SS0-1-G40-12-60	22.10	15.00	14.89	14.40	15.87	21.76	15.17	0.68	0.67	0.65	0.72	0.98	0.69
SS0-2-G40-12-60	26.53	15.00	14.89	14.40	15.87	21.76	15.17	0.57	0.56	0.54	0.60	0.82	0.57
Cont-1-G60-12-60	29.18	18.38	18.25	15.94	19.45	14.64	18.59	0.63	0.63	0.55	0.67	0.50	0.64
Cont-2-G60-12-60	27.85	18.38	18.25	15.94	19.45	14.64	18.59	0.66	0.66	0.57	0.70	0.53	0.67
SS20-1-G60-12-60	30.50	18.38	18.25	15.94	19.45	18.69	18.59	0.60	0.60	0.52	0.64	0.61	0.61
SS20-2-G60-12-60	28.29	18.38	18.25	15.94	19.45	18.69	18.59	0.65	0.64	0.56	0.69	0.66	0.66
SS10-1-G60-12-60	29.62	18.38	18.25	15.94	19.45	20.31	18.59	0.62	0.62	0.54	0.66	0.69	0.63
SS10-2-G60-12-60	30.95	18.38	18.25	15.94	19.45	20.31	18.59	0.59	0.59	0.52	0.63	0.66	0.60
SS0-1-G60-12-60	31.39	18.38	18.25	15.94	19.45	24.09	18.59	0.59	0.58	0.51	0.62	0.77	0.59
SS0-2-G60-12-60	32.27	18.38	18.25	15.94	19.45	24.09	18.59	0.57	0.57	0.49	0.60	0.75	0.58
Cont-1-G60-16-80	26.36	15.35	16.11	13.95	19.45	12.76	18.59	0.58	0.61	0.53	0.74	0.48	0.71
Cont-2-G60-16-80	27.60	15.35	16.11	13.95	19.45	12.76	18.59	0.56	0.58	0.51	0.70	0.46	0.67
SS20-1-G60-16-80	29.59	15.35	16.11	13.95	19.45	15.63	18.59	0.52	0.54	0.47	0.66	0.53	0.63
SS20-2-G60-16-80	25.11	15.35	16.11	13.95	19.45	15.63	18.59	0.61	0.64	0.56	0.77	0.62	0.74
SS10-1-G60-16-80	29.09	15.35	16.11	13.95	19.45	16.78	18.59	0.53	0.55	0.48	0.67	0.58	0.64
SS10-2-G60-16-80	29.34	15.35	16.11	13.95	19.45	16.78	18.59	0.52	0.55	0.48	0.66	0.57	0.63
SS0-1-G60-16-80	28.35	15.35	16.11	13.95	19.45	19.46	18.59	0.54	0.57	0.49	0.69	0.69	0.66
SS0-2-G60-16-80	30.33	15.35	16.11	13.95	19.45	19.46	18.59	0.51	0.53	0.46	0.64	0.64	0.61

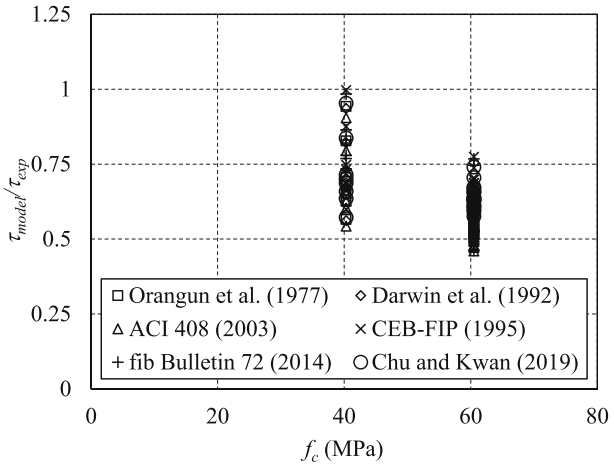

(a)

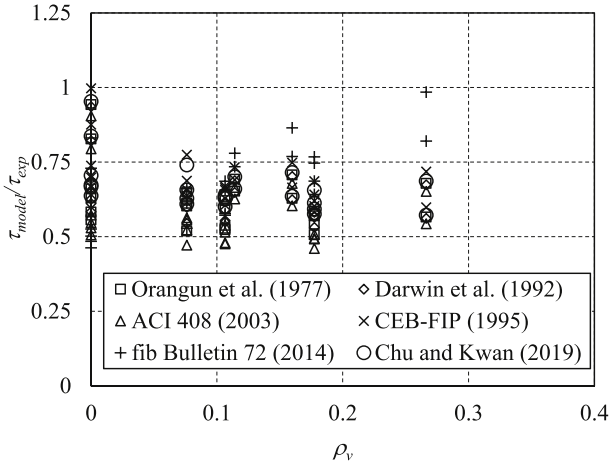

(b)

Fig. 12. Performance of existing models across: (a) f_c; and (b) ρ_v.

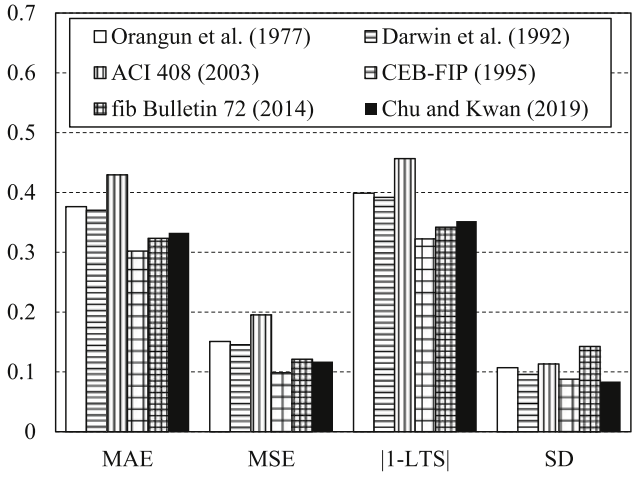

Fig. 13. Statistical performance of existing models.

noted that the setup of this regression function was designed to calibrate the influence of f_c and ρ_v. The influence of d_b is not calibrated in this study since the experimental test result did not show significant needs to recalibrate it. Therefore, the coefficient related to d_b in model proposed by fib Bulletin 72 (fib Bulletin 72, 2014) is directly adopted in this study.

$$\tau = \alpha\left(\frac{f_c}{25}\right)^{\beta}\left(\frac{d_b}{l_b}\right)^{0.45}\left(\frac{25}{d_b}\right)^{0.2}\left[\left(\frac{c_{\min}}{d_b}\right)^{0.25}\left(\frac{c_{\max}}{c_{\min}}\right)^{0.1}+\gamma\rho_v\right] \quad (7)$$

where α, β and γ are coefficient of the regression function.

From the regression analysis, α, β and γ are set to be 13.5, 1 and 1.45, respectively. Hence the proposed bond strength expression is given by Eq. (8).

$$\tau = 13.5\left(\frac{f_c}{25}\right)\left(\frac{d_b}{l_b}\right)^{0.45}\left(\frac{25}{d_b}\right)^{0.2}\left[\left(\frac{c_{\min}}{d_b}\right)^{0.25}\left(\frac{c_{\max}}{c_{\min}}\right)^{0.1}+1.45\rho_v\right] \quad (8)$$

The performance of the proposed model is assessed by estimating the bond strengths obtained from this experimental test. As evidenced from Fig. 14, most of the estimations are within the two 10% error margins and all the estimations are within the two 20% error margins. The MAE and MSE achieved by Eq. (8) are 0.06 and 0.01, respectively. These are significantly less compared to those of existing models. This means that the accuracy of the proposed model is higher than existing models. The |1-LTS| of the proposed model is 0.01 which indicates that LTS is very near to 1. Hence, the proposed model neither overestimated nor underestimated the bond strengths. The SD achieved by the proposed model is 0.07 and is the lowest when compared with existing models. This means that the proposed model is more consistent with the experimental test result. These performance indicators showed that the proposed model is accurate and reliable.

To further assess the proposed model, the model is used to estimate bond strengths of specimens confined with steel tube (Bamonte and Gambarova, 2007; Lee et al., 2012) and FRP wire jacket (Choi et al., 2014). Table 6 shows the details of specimens of the pull-out tests from previous research. It is noted that f_c is converted from the cylindrical concrete strength based on BS EN 1992-1-1 (British Standards Institution, 2014). For FRP wire jacket confinement, ρ_v was calculated by taking $f_y = \varepsilon_r E_{frp}$, where ε_r is the maximum radial strain of FRP measured in the experimental test; and E_{frp} is the elastic modulus of FRP. Besides, c_{min} is taken as c_{max} since the cross-section of the specimens are circular in shape. Fig. 15 shows the comparison between the results of previous experimental tests and estimations of the proposed model. It can be observed that the proposed model performed reasonably well with most of the estimations falls within the two 20% error margins. This means

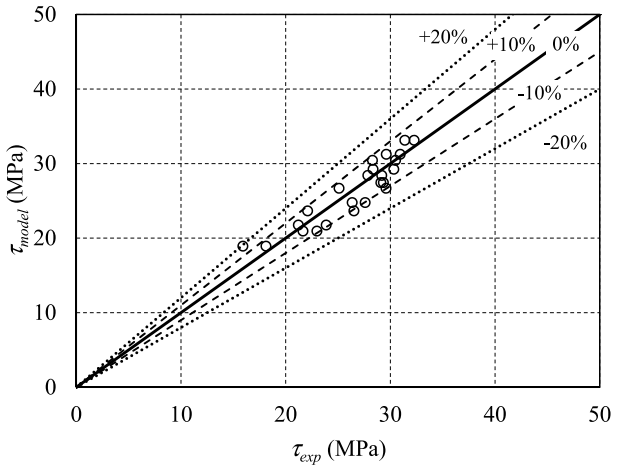

Fig. 14. Performance of proposed model against RSS confined specimens.

Table 6
Pull-out tests from previous research.

Reference	f_c (MPa)	d_b (mm)	l_b (mm)	c_{min} (mm)	ρ_v	τ (MPa)
Bamonte and Gambarova (2007)	47	5	27	20	0.488	31.12
Bamonte and Gambarova (2007)	47	5	27	20	0.488	33.01
Bamonte and Gambarova (2007)	47	5	27	20	0.488	30.42
Bamonte and Gambarova (2007)	47	12	80	48	0.508	26.63
Bamonte and Gambarova (2007)	47	12	64	48	0.508	24.70
Bamonte and Gambarova (2007)	47	12	64	48	0.508	29.80
Bamonte and Gambarova (2007)	47	18	96	72	0.452	24.37
Bamonte and Gambarova (2007)	47	18	96	72	0.452	24.78
Bamonte and Gambarova (2007)	47	18	96	72	0.452	24.98
Bamonte and Gambarova (2007)	47	26	138	104	0.469	23.17
Bamonte and Gambarova (2007)	47	26	138	104	0.469	24.77
Bamonte and Gambarova (2007)	47	26	138	104	0.469	23.37
Lee et al. (2012)	35	22	150	39	0.320	17.23
Lee et al. (2012)	35	22	150	39	0.320	16.39
Lee et al. (2012)	35	22	150	39	0.480	17.70
Lee et al. (2012)	35	22	150	39	0.480	17.60
Lee et al. (2012)	45	22	100	64	0.166	21.30
Lee et al. (2012)	45	22	100	64	0.249	21.50
Choi et al. (2014)	30	22	200	39	0.090	10.50
Choi et al. (2014)	30	22	200	39	0.078	10.64
Choi et al. (2014)	30	22	200	39	0.085	10.07
Choi et al. (2014)	30	22	200	39	0.038	11.43
Choi et al. (2014)	30	22	200	39	0.031	11.33
Choi et al. (2014)	30	22	200	39	0.042	11.57
Choi et al. (2014)	30	22	200	39	0.035	11.80
Choi et al. (2014)	30	22	200	39	0.053	11.98
Choi et al. (2014)	30	22	200	39	0.066	12.51
Choi et al. (2014)	45	22	200	39	0.066	12.77
Choi et al. (2014)	45	22	200	39	0.062	12.90
Choi et al. (2014)	45	22	200	39	0.079	13.03
Choi et al. (2014)	45	22	200	39	0.038	14.52
Choi et al. (2014)	45	22	200	39	0.043	14.04
Choi et al. (2014)	45	22	200	39	0.036	14.40
Choi et al. (2014)	45	22	200	39	0.041	14.75
Choi et al. (2014)	45	22	200	39	0.046	14.96
Choi et al. (2014)	45	22	200	39	0.068	15.20
Choi et al. (2014)	55	22	200	39	0.085	15.08
Choi et al. (2014)	55	22	200	39	0.082	15.25
Choi et al. (2014)	55	22	200	39	0.078	14.99
Choi et al. (2014)	55	22	200	39	0.081	17.27
Choi et al. (2014)	55	22	200	39	0.071	16.93
Choi et al. (2014)	55	22	200	39	0.080	16.96
Choi et al. (2014)	55	22	200	39	0.042	17.86
Choi et al. (2014)	55	22	200	39	0.063	17.67
Choi et al. (2014)	55	22	200	39	0.061	17.24

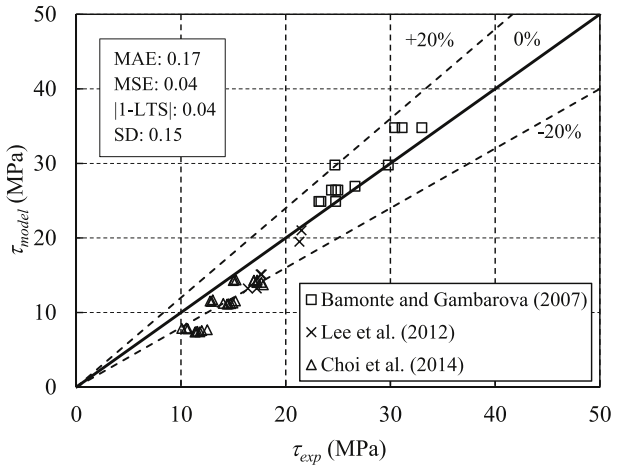

Fig. 15. Performance of proposed model against previous experimental tests.

that the proposed model captures the general influences of confinement on the bond strength. However, the estimations are less accurate compared to the estimations on RSS confinement. This is because of the differences in confinement mechanisms and the stress-strain behaviour of the confinement jackets.

7. Conclusion

This paper demonstrated the use of recycled steel as an active confinement to improve the bond strength between concrete and reinforcement steel. In this research, the tensile properties of the recycled steel were first tested. Subsequently, the recycled steel was made into confinement hoop and was installed on the specimens using mechanical prestressing to strengthen the specimens. A total of 24 pull-out tests were conducted in this research to assess the effect of the active recycled steel confinement on the bond strength. The parameters tested were concrete strength, confinement spacing and diameter of reinforcement bar. A new bond strength model was developed to consider the effect of the new active recycled steel confinement. The model was then compared against previous experimental test results.

From this research, the provision of confinement was found to be able to improve the bond strength and ductility of the bond. A new model was developed by modifying an existing model and calibrated to accommodate the influence of recycled steel confinement and concrete strength up to 60 MPa. Based on the findings presented in this paper, the following concluding remarks were made:

1. The lateral confinement pressure exerted by active RSS confinement effectively maintain the integrity of the concrete core. This improved the bond and changed the failure mode from sudden splitting to slip induced splitting.
2. This active RSS confinement can improve the bond strength between reinforcement steel and concrete by up to 40%. Active RSS confinement also can improve the maximum slip of reinforcement steel by up to 700%.
3. The bond strength and maximum slip improvement from active RSS confinement are affected by concrete strength and confinement ratio. Higher concrete strength will result in less improvement from active RSS confinement. Higher confinement ratio will result in more improvement from active RSS confinement.
4. A new expression for bond strength is proposed in this study to account of the variation in concrete strength and provision of active RSS confinement. Most of the estimations on RSS confined pull-out tests using this model are within 10% error and the average error of the estimation is 6%.

While many findings have been reported in this paper, it is recommended to investigate further in future research especially on the potential variation of bond strength due to changes in cement paste volume (Chu, 2019) and type of concrete (Zhang et al., 2022).

CRediT authorship contribution statement

Muhd Fauzy Sulaiman: Investigation, Conceptualization, Writing – original draft. **Chee-Loong Chin:** Validation, Writing – review & editing. **Chau-Khun Ma:** Resources, Funding acquisition. **Abdullah Zawawi Awang:** Project administration. **Wahid Omar:** Supervision.

Declaration of competing interest

The authors declare that they have no known competing financial interests or personal relationships that could have appeared to influence the work reported in this paper.

Data availability

Data will be made available on request.

Acknowledgement

The authors gratefully acknowledge the financial support for this research from the Universiti Teknologi Malaysia Grant no: [Q.J130000.2451.09G87], [Q.J130000.3851.20J22] and industrial contract grant with [R.J130000.7651.4C540].

List of Symbol

τ = bond strength
α = first coefficient alpha of the regression function
β = second coefficient of the regression function
γ = third coefficient of the regression function
$\tau_{average}$ = average bond strength
$\tau_{cont,average}$ = average bond strength of unconfined specimen
τ_{exp} = experimental bond strength
τ_{model} = estimated bond strength
ε_r = maximum radial strain of FRP measured in the experimental test
ρ_v = confinement ratio
$\overline{\tau}_{exp}$ average of τ_{exp}
$\overline{\tau}_{model}$ = average of τ_{model}
A_b = cross-sectional area of reinforcement bar
A_{tr} = cross-sectional area of each stirrup
c = $\min(c_s, c_y, c_s/2)$
c_{max} = $\max(\min(c_x, c_s/2), c_y)$
c_{min} = $\min(c_y, c_s/2)$
c_s = distance between reinforcement bars
c_x = side concrete cover
c_y = bottom concrete cover
D = diameter of concrete
d_b = diameter of reinforcement bar
E_{frp} = elastic modulus of FRP
f_c = concrete cubic compressive strength
f_y = yield stress of recycled steel straps
K_{tr} = $n_{st}a_{st}/(s\ d_b\ n_b)$
l_d = bond length of reinforcement bar
LTS = linear trend slope
MAE = mean absolute error
MSE = mean squared error
N = Number of estimations
n_b = number of individual anchored bars or pairs of lapped bars
n_{st} = number of legs of a stirrup which crosses the potential splitting failure plane
P_{max} = maximum pull-out load
s = centre spacing between stirrups or confinement
s_{cl} = clear spacing between confinement
SD = standard deviation
t = thickness of recycled steel straps
t_d = factor for the effects of bar size
t_r = factor for the effects of relative rib area
V_c = volume of concrete
V_s = volume of recycled steel straps
w = width of recycled steel straps
x = volume of fibre(length of fibre /diameter of fibre)

References

ACI 408, ACI R408-03: Bond and Development of Straight Reinforcing Bars in Tension, 2003. American Concrete Institute, Farmington Hills, Mich.

Alagusundaramoorthy, P., Harik, I.E., Choo, C.C., 2003. Flexural behavior of R/C beams strengthened with carbon fiber reinforced polymer sheets or fabric. J. Compos. Construct. 7 (4), 292–301. https://doi.org/10.1061/(ASCE)1090-0268(2003)7:4(292), 2003.

ASTM C150/C150M-20, 2020. Standard Specification for Portland Cement, West Conshohocken, PA.

Awang, A.Z., 2013. Stress-strain Behaviour of High-Strength Concrete with Lateral Pre-tensioning Confinement. Universiti Teknologi Malaysia.

Bamonte, P.F., Gambarova, P.G., 2007. High-bond bars in NSC and HPC: study on size effect and on the local bond stress-slip law. J. Struct. Eng. 133 (2), 225–234. https://doi.org/10.1061/(ASCE)0733-9445(2007)133:2(225), 2007.

Bandelt, M.J., Frank, T.E., Lepech, M.D., Billington, S.L., 2017. Bond behavior and interface modeling of reinforced high-performance fiber-reinforced cementitious composites. Cement Concr. Compos. 83 (2017), 188–201. https://doi.org/10.1016/j.cemconcomp.2017.07.017.

British Standards Institution, 2009. BS EN 12390-3:2009. Testing Hardened Concrete. Part 3: Compressive Strength of Test Specimens. BSI.

British Standards Institution, 2014. Eurocode 2: Design of Concrete Structures. Part 1-1: General Rules and Rules for Buildings. BS EN 1992-1-1:2004, London.

CEB-FIP working group on high strength/high performance concrete, high strength concrete: state of the art report, CEB Bulletin No. 197, 1990.

CEB-FIP working group on high strength/high performance concrete, high performance concrete: recommended extensions to the model code 90: research needs. CEB Bulletin No 228, 1995.

Chan, J., Bachmann, C., Haas, C., 2020. Potential economic and energy impacts of substituting adaptive reuse for new building construction: a case study of Ontario. J. Clean. Prod. 259 (2020) https://doi.org/10.1016/j.jclepro.2020.120939, 120939.

Chin, C.-L., Ma, C.-K., Awang, A.Z., Omar, W., Kueh, A.B.H., 2018. Stress–strain evaluation of steel-strapped high-strength concrete with modified self-regulating end clips. Struct. Concr. 19 (4), 1036–1048. https://doi.org/10.1002/suco.201700134, 2018.

Chin, C.-L., Ma, C.-K., Tan, J.-Y., Ong, C.-B., Awang, A.Z., Omar, W., 2019a. Review on development of external steel-confined concrete. Construct. Build. Mater. 211, 919–931. https://doi.org/10.1016/j.conbuildmat.2019.03.295, 2019.

Chin, C.-L., Ma, C.-K., Awang, A.Z., Tan, J.-Y., Ong, C.-B., Omar, W., 2019b. Confining stress path dependent stress-strain model for pre-tensioned steel-confined concrete. Eng. Struct. 201 (2019), 109769 https://doi.org/10.1016/j.engstruct.2019.109769.

Chin, C.-L., Ong, C.-B., Tan, J.-Y., Ma, C.-K., Awang, A.Z., Omar, W., 2020. Confinement-concrete interaction in pre-tensioned partial steel-confined concrete. Structures 23 (2020), 751–765. https://doi.org/10.1016/j.istruc.2019.12.006.

Choi, E., Chung, Y.-S., Park, C., Kim, D.J., 2013. Seismic performance of circular RC columns retrofitted with prefabricated steel wrapping jackets. Mag. Concr. Res. 65 (23), 1429–1440. https://doi.org/10.1680/macr.13.00177, 2013.

Choi, E., Cho, B.-S., Jeon, J.-S., Yoon, S.-J., 2014. Bond behavior of steel deformed bars embedded in concrete confined by FRP wire jackets. Construct. Build. Mater. 68 (2014), 716–725. https://doi.org/10.1016/j.conbuildmat.2014.06.092.

Chu, S.H., 2019. Effect of paste volume on fresh and hardened properties of concrete. Construct. Build. Mater. 218, 284–294. https://doi.org/10.1016/j.conbuildmat.2019.05.131, 2019.

Chu, S.H., Kwan, A.K.H., 2018. A new method for pull out test of reinforcing bars in plain and fibre reinforced concrete. Eng. Struct. 164 (2018), 82–91. https://doi.org/10.1016/j.engstruct.2018.02.080.

Chu, S.H., Kwan, A.K.H., 2019. A new bond model for reinforcing bars in steel fibre reinforced concrete. Cement Concr. Compos. 104 (2019), 103405 https://doi.org/10.1016/j.cemconcomp.2019.103405.

Chu, S.H., Kwan, A.K.H., 2021. Crack mitigation utilizing enhanced bond of rebars in SFRC. Structures 33 (2021), 4141–4147. https://doi.org/10.1016/j.istruc.2021.06.095.

Chu, S.H., Li, L.G., Kwan, A.K.H., 2018. Fibre factors governing the fresh and hardened properties of steel FRC. Construct. Build. Mater. 186 (2018), 1228–1238. https://doi.org/10.1016/j.conbuildmat.2018.08.047.

Conejos, S., Langston, C., Smith, J., 2014. Designing for better building adaptability: a comparison of adaptSTAR and ARP models. Habitat Int. 41, 85–91. https://doi.org/10.1016/j.habitatint.2013.07.002, 2014.

Darwin, D., McCabe, S.L., Idun, E.K., Schoenekase, S.P., 1992. Development length criteria: bars not confined by transverse reinforcement. ACI Struct. J. 89 (6) https://doi.org/10.14359/4158, 1992.

Fib Bulletin 72, Bond and Anchorage of Embedded Reinforcement: Background to the Fib Model Code for Concrete Structures 2010, 2014. fib-Fédération internationale du béton, Germany.

Gong, Y., Shan, Y., Liu, X., Ding, F., Wu, Y., 2021. Static bond behavior between corroded corner steel bar and concrete under the hoop confinement of CFRP sheets. Compos. Struct. 276 (2021), 114589 https://doi.org/10.1016/j.compstruct.2021.114589.

Hamad, B.S., Ali, A.Y.H., Harajli, M.H., 2005. Effect of fiber-reinforced polymer confinement on bond strength of reinforcement in beam anchorage specimens. J. Compos. Construct. 9 (1), 44–51. https://doi.org/10.1061/(ASCE)1090-0268(2005)9:1(44), 2005.

Iacovidou, E., Purnell, P., 2016. Mining the physical infrastructure: opportunities, barriers and interventions in promoting structural components reuse. Sci. Total Environ. 557–558 (2016), 791–807. https://doi.org/10.1016/j.scitotenv.2016.03.098.

Kaklauskas, G., Ramanauskas, R., Jakubovskis, R., 2017. Mean crack spacing modelling for RC tension elements. Eng. Struct. 150, 843–851. https://doi.org/10.1016/j.engstruct.2017.07.090, 2017.

Lee, J.Y., Kim, T.Y., Kim, T.J., Yi, C.K., Park, J.S., You, Y.C., Park, Y.H., 2008. Interfacial bond strength of glass fiber reinforced polymer bars in high-strength concrete. Compos. B Eng. 39 (2), 258–270. https://doi.org/10.1016/j.compositesb.2007.03.008, 2008.

Lee, H., Choi, E., Cho, S.-C., Park, T., 2012. Bond and splitting behaviour of reinforced concrete confined by steel jackets without grouting. Mag. Concr. Res. 64 (3), 225–237. https://doi.org/10.1680/macr.2012.64.3.225, 2012.

Lim, J.C., Ozbakkaloglu, T., 2014. Unified stress-strain model for FRP and actively confined normal-strength and high-strength concrete. J. Compos. Construct. 19 (4), 04014072 https://doi.org/10.1061/(ASCE)CC.1943-5614.0000536, 2014.

Ma, C.-K., Awang, A.Z., Garcia, R., Omar, W., Pilakoutas, K., 2016a. Behaviour of over-reinforced high-strength concrete beams confined with post-tensioned steel straps – an experimental investigation. Struct. Concr. 17 (5), 768–777. https://doi.org/10.1002/suco.201500062, 2016.

Ma, C.K., Awang, A.Z., Garcia, R., Omar, W., Pilakoutas, K., Azimi, M., 2016b. Nominal curvature design of circular HSC columns confined with post-tensioned steel straps. Structures 7 (2016), 25–32. https://doi.org/10.1016/j.istruc.2016.04.002.

Mander, J.B., Priestley, M.J.N., Park, R., 1988. Theoretical stress-strain model for confined concrete. J. Struct. Eng. 114 (8), 1804–1826. https://doi.org/10.1061/(ASCE)0733-9445(1988)114:8(1804), 1988.

Moghaddam, H., Samadi, M., Pilakoutas, K., Mohebbi, S., 2010. Axial compressive behavior of concrete actively confined by metal strips. part A: experimental study, Materials and Structures 43 (10), 1369–1381. https://doi.org/10.1617/s11527-010-9588-6, 2010.

Olivier, J.G.J., Peters, J.A.H.W., Janssens-Maenhout, G., 2012. Trends in Global CO2 Emissions. 2012 Report. Netherlands Environmental Assessment Agency PBL, Den Haag (Netherlands); Institute for Environment and Sustainability IES, European Commission; Joint Research Centre JRC, Ispra (Italy), pp. 1–40.

Ong, C.-B., Chin, C.-L., Ma, C.-K., Tan, J.-Y., Awang, A.Z., Omar, W., 2022. Seismic retrofit of reinforced concrete beam-column joints using various confinement techniques: a review. Structures 42, 221–243. https://doi.org/10.1016/j.istruc.2022.05.114, 2022.

Orangun, C.O., Jirsa, J.O., Breen, J.E., 1977. A reevaulation of test data on development length and splices. ACI Journal Proceedings 74 (3). https://doi.org/10.14359/10993, 1977.

Samani, A.K., Attard, M.M., 2012. A stress–strain model for uniaxial and confined concrete under compression. Eng. Struct. 41 (2012), 335–349. https://doi.org/10.1016/j.engstruct.2012.03.027.

Sulaiman, M.F., Ma, C.-K., Apandi, N.M., Chin, S., Awang, A.Z., Mansur, S.A., Omar, W., 2017. A review on bond and anchorage of confined high-strength concrete. Structures 11, 97–109. https://doi.org/10.1016/j.istruc.2017.04.004, 2017.

Torre-Casanova, A., Jason, L., Davenne, L., Pinelli, X., 2013. Confinement effects on the steel–concrete bond strength and pull-out failure. Eng. Fract. Mech. 97, 92–104. https://doi.org/10.1016/j.engfracmech.2012.10.013, 2013.

United Nations Environment Programme, 2020. Global Status Report for Buildings and Construction: towards a Zero-Emission, Efficient and Resilient Buildings and Construction Sector. Nairobi, 2020.

Wang, Y., Chen, G., Wan, B., Han, B., Ran, J., 2021. Axial compressive behavior and confinement mechanism of circular FRP-steel tubed concrete stub columns. Compos. Struct. 256 (2021), 113082 https://doi.org/10.1016/j.compstruct.2020.113082.

Wei, W., Liu, F., Xiong, Z., Lu, Z., Li, L., 2019. Bond performance between fibre-reinforced polymer bars and concrete under pull-out tests. Construct. Build. Mater. 227 (2019), 116803 https://doi.org/10.1016/j.conbuildmat.2019.116803.

Xiong, Z., Wei, W., He, S., Liu, F., Luo, H., Li, L., 2021. Dynamic bond behaviour of fibre-wrapped basalt fibre-reinforced polymer bars embedded in sea sand and recycled aggregate concrete under high-strain rate pull-out tests. Construct. Build. Mater. 276 (2021), 122195 https://doi.org/10.1016/j.conbuildmat.2020.122195.

Yang, Y., Xue, Y., Wang, N., Yu, Y., 2019. Experimental and numerical study on seismic performance of deficient interior RC joints retrofitted with prestressed high-strength steel strips. Eng. Struct. 190 (2019), 306–318. https://doi.org/10.1016/j.engstruct.2019.03.096.

Zhang, D., Li, N., Li, Z.-X., Xie, L., 2020. Experimental investigation and confinement model of composite confined concrete using steel jacket and prestressed steel hoop. Construct. Build. Mater. 256 (2020), 119399. https://doi.org/10.1016/j.conbuildmat.2020.119399.

Zhang, J., Tao, X., Li, X., Zhang, Y., Liu, Y., 2022. Analytical and experimental investigation of the bond behavior of confined high-strength recycled aggregate concrete. Construct. Build. Mater. 315 (2022), 125636 https://doi.org/10.1016/j.conbuildmat.2021.125636.